Case Studies in Thermal Engineering 51 (2023) 103642

Contents lists available at ScienceDirect

Case Studies in Thermal Engineering

journal homepage: www.elsevier.com/locate/csite

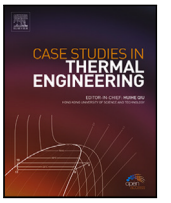

Computational analysis of radiative heat transfer due to rotating tube in parabolic trough solar collectors with Darcy Forchheimer porous medium

B.K. Sharma [a,*], Anup Kumar [a], Bandar Almohsen [b], Unai Fernandez-Gamiz [c]

[a] Department of Mathematics, Birla Institute of Technology and Science, Pilani, Rajasthan, India
[b] Department of Mathematics, College of Science, King Saud University, Riyadh 11451, Saudi Arabia
[c] Department of Nuclear and Fluid Mechanics, University of the Basque Country (UPV/EHU), Nieves Cano 12, 01006 Vitoria-Gasteiz, Spain

ARTICLE INFO

Keywords:
Rotating tube
Darcy Forchheimer porous medium
Riga surface
Hybrid nanofluid
Solar radiation
Heat transfer

ABSTRACT

This attempt numerically investigates the heat transfer in parabolic trough solar collectors due to the rotating tube for the hybrid nanofluid flow over the Riga surface with Darcy Forchheimer's porous medium under the effect of solar radiation. The influences of viscous dissipation and Joule heating are also considered. Equations governing the fluid flow are non-dimensionalized by implementing appropriate similarity variables. The resulting non-dimensionalized ordinary differential equations are solved using the shooting technique with Adam Bashforth and Adam Moulten's fourth-order numerical approach. The numerical outcomes for various influential physical parameters regarding the fluid velocity, temperature, Nusselt number, and entropy generation are presented in graphical form. It is observed that the thermal profile escalates with the higher values of Reynold's number, modified magnetic field parameter, and Prandtl number. Also, the Nusselt number diminishes with augmenting values of the Eckert number, modified magnetic field parameter, Forchheimer number, and Darcy number. The optimization of heat transfer in parabolic trough collectors is essential to improve the performance of solar collectors. The concentrated solar power technology is adequate for storing radiation energy in higher amounts.

1. Introduction

Solar energy is an effective solution for addressing current energy requirements. It reduces the use of fossil fuels in energy consumption and is safe for our environment. Concentrated solar power technology efficiently stores the Sun's radiation energy in possibly more significant amounts. This technology uses a parabolic trough, which reflects the incoming solar radiation about a fixed axis towards the bottom perimeter of the receiver tube. Energy from the concentrated solar radiation is absorbed by the receiver tube, also known as the absorber tube. The absorber tube is housed in an envelope of glass to protect the thermal losses from the environment. The fluid working in a parabolic trough receiver plays a significant role in the overall performance of the collector [1,2]. Jianfeng et al. [3] introduced heat transfer performance under the effect of concentrated solar radiation in parabolic trough solar collectors. A computational model of the heat transfer due to concentrated solar radiation in the receiver tube was made by Chen et al. [4]. Lipinski et al. [5] discussed the advances, problems, and prospectives in thermochemical energy heat transfer systems and high-temperature solar thermal collectors.

* Corresponding author.
E-mail addresses: bhupen_1402@yahoo.co.in (B.K. Sharma), yadavanupbalwan1996@gmail.com (A. Kumar), balmohsen@ksu.edu.sa (B. Almohsen), unai.fernandez@ehu.eus (U. Fernandez-Gamiz).

https://doi.org/10.1016/j.csite.2023.103642
Received 7 August 2023; Received in revised form 5 October 2023; Accepted 16 October 2023
Available online 17 October 2023

Riga plate is usually employed to enhance the fluid's thermophysical characteristics and prevent mechanical energy loss. Riga plate is an electromagnetic actuator constructed from permanent electrodes and magnets. The strength of the magnetic and electric field has a specific external element called Lorentz force that controls the fluid flow, which regulates the fluid flow. Pantokratoras and Magyari [6] incorporated the Riga surface in the boundary layer free convection flow. The electrically conductive nanofluid flow over the Riga surface was analyzed by Ayub et al. [7]. Ahmad et al. [8] performed the analysis of heat transfer over Riga surface in the nanofluid flow. The flow of Walters-B fluid over the Riga plate was described by Shafiq et al. [9]. Rasool et al. [10] analyzed the heat transfer due to the second-grade nanofluid flow passing across Riga surface. The description of gyrotactic microorganisms swimming in a Maxwell nanofluid past Riga surface was given by Ramesh et al. [11]. Asogwa et al. [12] investigated the heat transfer due to the Casson fluid with heat absorption along an inclined Riga plate. Sharma et al. [13] done the study of heat transfer by magnetohydrodynamic fluid flow with the thermophoretic diffusion and Brownian motion effects. Moreover, Sharma et al. [14] also studied the magnetohydrodynamic slip flow of blood through tapered multi-stenosed arteries. Ghandhi et al. [15] did the analysis of magnetically targeted drug delivery through bell-shaped arteries. Sharma et al. [16] investigated the interaction of an incompressible electro-magnetohydrodynamic Jeffrey nanofluid flow past a non-linear elongation surface. The low Prandtl number for Maxwell fluid treated with hydromagnetic slip flow and heat transfer was analyzed by Sultana et al. [17]. Marangoni stagnation point in thermosol Nanofluid flow of GO-MoS_2/water on a stretched sheet with an inclined magnetic field was discussed by [18].

The collector's efficiency is enhanced by minimizing the average difference of temperature in the collector surface and the working fluid. Notably, porous materials accelerates the heat transfer by increasing the contact between the collector surface and the working fluid, which creates a thinner hydrodynamic boundary layer between the fluid and surface of the collector [19]. The thermal efficiency of a receiver with porous medium under concentrated incidence of solar radiation was investigated by Wang et al. [20]. Wang et al. [21] also discussed thermophysical models by the mixture as the input gas with porous medium in the receiver tube for heat transfer. The radiation–convection heat transmission in the porous medium for solar heat exchangers was studied by Soltani et al. [22]. Beg et al. [23] computed the heat transfer through absorber in the porous medium using the radiative differential approximation. The survey of Rashidi et al. [24] examined the heat transfer in solar heat exchangers or sun heaters comprised of porous medium. The investigation of heat transfer in the solar thermochemical reactor with the porous medium was done by Logou et al. [25]. Changes in effective thermal conductivity due to porous materials by considering the effects of heat radiation were evaluated by Luo et al. [26]. Magnetohydrodynamic mixed convective unsteady flow in the presence of Darcy–Forchheimer porous medium was investigated by Sharma et al. [27]. Thermodynamic investigation of solar water heater employing Titanium oxide/oil nanofluid combined with the porous medium was done by [28]. The hybrid nanofluid flow with Darcy–Forchheimer porous medium across an infinite porous disk was investigated by Mohanty et al. [29].

Most of the nanofluids associated with direct absorption solar collectors were mono nanofluids. Nevertheless, mono-nanofluids have significant drawbacks in certain areas. For example, carbon nanotubes have exceptionally higher thermal conductivities and remarkable optical properties, and they have some disadvantages because the absorption spectrum of these nanoparticles is predominantly in the visible spectrum, with poor absorption in the near-infrared region [30]. To overcome these obstacles, the researchers proposed hybrid nanofluids, and multiple types of nanoparticles are dissolved in conventional fluid to prepare hybrid nanofluids. Numerous attempts indicate that hybrid nanofluids have more incredible abilities for enhancing heat transfer than mono-nanofluids, as discussed in the survey by Ahmadi et al. [31]. Xiong et al. [32] presented the review article for on thermal performance enhancement of the parabolic trough solar collectors by introducing various types of hybrid nanofluids. The review paper by Hu et al. [33] described the heat transfer due to the different types of hybrid nanofluids and observed that hybrid nanofluids have better efficiency than mono-nanofluids and fluids. Kumar et al. [34] examined the performance of ferromagnetic hybrid nanofluids in enhancement of heat transfer . The efficiency of hybrid nanoparticles Al_2O_3/MWCNT and Therminol-VPI base fluid are superior for the stability and heat transfer analyzed from the literature by Adun et al. [35]. The solar collector's thermal efficiency rises by 10.42% for using Al_2O_3/MWCNT and terminal-VPI hybrid nanofluid with direct normal irradiance between 700 and 1000 W/m^2 was concluded from the study of Abid et al. [36]. The review article by Tiwari et al. [37] declares that the efficiency of hybrid nanofluid is 0.6% greater than MWCNT-oil based nanofluid, 1.98% greater than Al_2O_3-oil based nanofluids, and 2.58% greater than pure terminal-VPI. Ghandhi et al. [38] analyzed the entropy generation in the suspension of Au/Al_2O_3 in the magnetohydrodynamic blood flow. Tavakoli [39] determined the optimal direction to store higher thermal energy in more significant amounts utilizing water and Therminol VP-I. It is discovered that at low temperatures, water is the more economical option, whereas industrial oil should be used at higher temperatures. Also, from the remarks of the literature [40–42], it is concluded that the use of MWCNT/Al_2O_3 hybrid nanofluids increase the performance of the thermal energy systems. Hydrothermofluidic characteristics sensitive to low and intermediate Prandtl numbers for Oldroyd B fluid were investigated by Gope et al. [43].

All irreversible thermofluidic processes result in a loss of efficiency. In practice, the amount of these irreversibilities is calculated via entropy generation. It is preferable to slow down the entropy generation rate to enhance the storage of available energy in the thermodynamic systems. Parvin et al. [44] examined the entropy formation due to forced convection heat transfer in a solar collector with direct absorption. A numerical simulation of a flat plate solar collector with laminar conjugated heat transfer by mixed convection was done by Charjouei et al. [45]. Entropy formation in Casson cross micropolar nanofluid with the thermal radiation for the three-dimensional unsteady magnetohydrodynamic flow was computed by Nayak et al. [46]. Wang et al. [47] simulated the single two-phase closed thermosyphon nanofluid flow to investigate its thermal performance. Sharma et al. [48] numerically studied the entropy produced in the fluid flow driven by magnetohydrodynamic effects. Kumawat et al. [49] discussed entropy formation in the magnetohydrodynamic blood flow in a porous curve-shaped artery. A thermal model based on three-dimensional Finite Volume with non-uniform solar heat flux was devised by Goyal and Reddy [50]. Entropy generation and heat transfer in the

Jeffrey nanofluid flow under the effect of solar radiation were investigated by Sharma et al. [51]. Entropy simulation in a hybrid water-EG nano liquid flow using magnetohydrodynamic was done by Sen et al. [52]. The irreversibility of magnetohydrodynamic convective hybrid nanofluid flow due to a rotating disk with nonlinear thermal radiation was examined by Mohanty et al. [53].

Previous investigations deal with thermal energy storage due to static laminar fluid flow through the absorber tube in parabolic trough solar collectors using conventional fluids. An attempt has yet to be made to analyze the entropy generation and heat transfer in parabolic trough solar collectors due to hybrid nanofluid flow under the influence of the rotating tube with Darcy Forchheimer porous medium along the Riga surface. Hence, this study investigates the entropy generation and heat transfer for enhancing thermal energy storage of parabolic trough collectors affected by the following physical situations.

- This attempt analyzes the heat transfer in parabolic trough solar collectors due to hybrid nanofluid flow under the influence of the rotating tube.
- A homogeneous mixture of Al_2O_3 and MWCNT hybrid nanoparticles and Therminol-VPI synthetic fluid is considered as the heat transfer fluid.
- The influences of viscous dissipation, Ohmic heating, Darcy Forchheimer porous medium, and Riga surface (Electromagneto-hydrodynamic) are also taken in the investigation.
- Adam Bashforth and Adam Moulten's fourth-order numerical approach is implemented with the shooting technique to solve non-dimensionalized governing ordinary differential equations.
- Entropy generation in heat transfer for parabolic trough solar collectors due to rotating tube for the hybrid nanofluid flow is also investigated.

The computational analysis of radiative heat transfer in parabolic trough solar collectors with a rotating tube and Darcy-Forchheimer porous medium using hybrid nanofluids holds excellent importance in Case Studies in Thermal Engineering. This research addresses the critical issues for storing renewable solar energy due to parabolic trough solar collectors in thermal engineering. The parabolic trough collectors are vital for harnessing solar power efficiently, and enhancing their performance is crucial for advancing clean energy solutions. Overall, this research bridges theory and application, offering tangible benefits to thermal engineering. It advances the design and optimization of solar thermal systems, contributing to sustainable and clean energy sources.

2. Physical assumptions

Steady-state incompressible flow in a laminar pattern for hybrid nanofluid flowing in the absorber with inserted rotating tube is considered under the effect of viscous dissipation, Ohmic heating, Darcy Forchheimer porous medium, and solar radiation. It is assumed that the solar radiations on the receiver tube are concentrated by the parabolic trough. The receiver tube and inner tube temperatures are initially taken as constant with a constant rotation of the inner tube. In general, the vector product $F = J \times B$ determines the Lorentz force, where J indicates the induced density of the electric current, and the magnetic field induced is given by B. According to Ohm's law, the equation $J = \sigma(E + V \times B)$ determines the current density, where E stands for electric field and V for velocity of fluid, respectively. The desired electric current density can be achieved for fluid flows with high electrical conductivity without external electric fields. The current density achieved by the magnetic field of 1 T applied is enough to gain control (MHD flow control), and in this scenario, the Lorentz force is $F = J \times B \approx \sigma(V \times B)B$. However, for fluids with low electrical conductivities like 10 S/m or less, the current density produced by magnetic fields of several Teslas without an electric field is insufficient and is negligibly too small. The flow field needs an external electric field to control the low electrical conductive fluid flows. In that case, the Lorentz force is defined as $F = J \times B \approx \sigma(E \times B)$.

The applied electric field and magnetic field are in the spanwise direction r normal to the wall for the Riga plate. Because of the stripwise character of the plate, significant spanwise changes in F occur close to its surface, but these variations quickly diminish as the distance r increases. The average of the force density $F = F_{ex}$ along the spanwise coordinate z converts into a function exponentially decreasing in the direction r, which is given by:

$$F = \frac{\pi J M}{8\tilde{\rho}} exp\left(-\frac{\pi}{a_0} r\right)$$

where a_0 denotes the width of the permanent magnets and electrodes, M (Tesla) is the strength of the magnets, and $J\,(\mathrm{A/m^2})$ represents the current density applied by the electrodes. This equation describes the force experienced by charged particles or elements due to electromagnetic interactions. It gives the precise computation of the Lorentz force and the exponential term describes the variation in Lorentz force density within the boundary layer of the fluid. This equation incorporates the fundamental electromagnetism concepts and beneficial in understanding complex electromagnetic interactions. It is an extremely useful tool for explaining and modeling the behavior of electromagnetic forces (see Fig. 1).

According to the assumptions mentioned above, the following equations govern the viscous incompressible hybrid nanofluid flow in the boundary layer [54,55]:

Momentum equation

$$U\frac{\partial U}{\partial R} = \nu_{hnf}\left(\frac{\partial^2 U}{\partial R^2} + \frac{1}{R}\frac{\partial U}{\partial R} - \frac{U}{R^2}\right) - \frac{\pi J M}{\rho_{hnf}} exp(-\frac{\pi}{a_0} R) - \nu_{hnf}\frac{U}{K_1} - \frac{C_b}{\sqrt{K_1}}U^2, \tag{1}$$

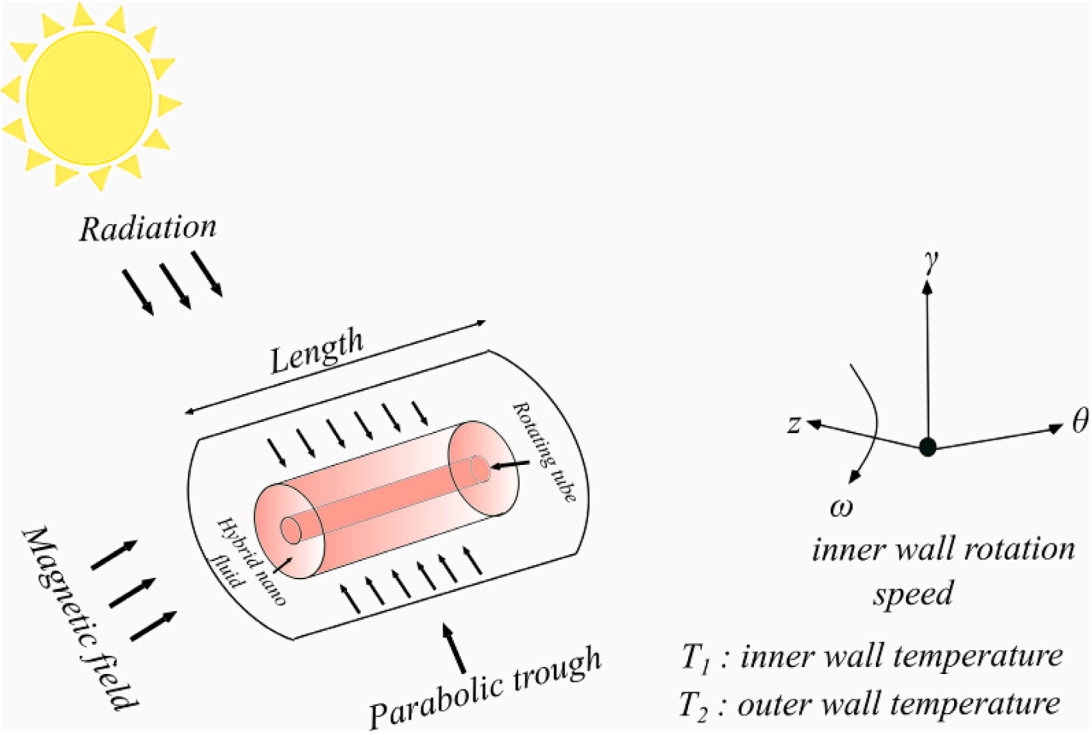

Fig. 1. Physical geometry of the solar collector.

Table 1
Physical properties of the nanoparticles and base fluid.

Physical properties	Al_2O_3	MWCNT	Therminol-VPI
Density [ρ (kg/m^3)]	3970	1600	938
Heat capacitance [C_p (J/kg K)]	765	796	1970
Thermal conductivity [κ (W/m K)]	40	3000	0.118

Energy equation

$$(\rho C_p)_{hnf} U \frac{\partial T}{\partial R} = \frac{k_{hnf}}{R}\frac{\partial}{\partial R}\left(R\frac{\partial T}{\partial R}\right) + \mu_{hnf}\left(\frac{\partial U}{\partial R} - \frac{U}{R}\right)^2 - \frac{1}{R}\frac{(R\partial q_R)}{\partial R} + \frac{\pi J M}{\rho_{hnf}} exp(-\frac{\pi}{a_0}R)U. \quad (2)$$

where,

$$q_R = -\frac{4\sigma_e}{3\beta_R}\frac{\partial T^4}{\partial R}$$

is the expression for the non-linear radiation approximated by Rosseland approximation.

And,

$$T^4 \cong 4T_2^3 T - 3T_2^4$$

T^4 is expanded about T_2 using Taylor series.

Boundary conditions:

$$R = r_1 : \quad U(R) = \omega r_1, \quad T = T_1,$$
$$R = r_2 : \quad U(R) = 0, \quad T = T_2.$$

Physical properties of the Aluminum-Oxide (Al_2O_3) nanoparticles and multi-walled carbon nanotubes (MWCNT) and Therminol-VPI are given in the Table 1.

Expressions for the evaluation of thermophysical properties of hybrid nanofluids are given by: Dynamic viscosity

$$\mu_{hnf} = \frac{\mu_f}{(1-\phi_1)^{2.5}(1-\phi_2)^{2.5}},$$

Density

$$\rho_{hnf} = \phi_1\rho_1 + \left(1-\phi_1\right)\left[\left(1-\phi_2\right)\rho_f + \phi_2\rho_2\right],$$

Specific heat capacity

$$(c_p)_{hnf} = (1-\phi_1)[\left(1-\phi_2\right)(c_p)_f + \phi_2(c_p)_2] + \phi_1(c_p)_1,$$

Thermal conductivity

$$k_{hnf} = \left(k_{nf}\right) \times \frac{k_1 + 2k_{nf} - 2\phi_1\left(k_{nf}-k_1\right)}{\phi_1(k_{nf}-k_1) + k_1 + 2k_{nf}},$$

where,

$$k_{nf} = \frac{k_2 + 2k_f - 2\phi_2\left(k_f - k_2\right)}{k_2 + 2k_f + \phi_2\left(k_f - k_2\right)} \times \left(k_f\right),$$

3. Similarity transformations

$$r = \frac{R}{r_2}, u = \frac{U}{\omega r_1}, \eta = \frac{r_1}{r_2}, \theta = \frac{T-T_2}{T_1-T_2},$$

where r_2, r_1, ω, T_2, and T_1 are the external tube's radius, the internal tube's radius, the internal tube's constant velocity of the rotation, the internal tube's surface temperature, and the external tube's surface temperature, respectively. As a result, the dimensionless governing equations are:

Non-dimensionalized momentum equation:

$$\frac{\partial^2 u(r)}{\partial r^2} + \frac{1}{r}\frac{\partial u(r)}{\partial r} - \frac{1}{r^2}u(r) - Re\frac{S_1}{S_2}u(r)\frac{\partial u(r)}{\partial r} - \frac{M_0}{S_2}exp(-\beta r) - Dau(r) - \frac{S_2}{S_1}F_r u^2(r) = 0, \tag{3}$$

Non-dimensionalized energy equation:

$$\frac{\partial^2\theta(r)}{\partial r^2} + \frac{1}{r}\frac{\partial\theta(r)}{\partial r} + EcPr\frac{S_2}{S_4}\left\{\frac{\partial u(r)}{\partial r} - \frac{1}{r}u(r)\right\}^2 + \frac{4Rd}{3S_4}\frac{1}{r}\frac{\partial(r\theta(r))}{\partial r} - PrRe\frac{S_3}{S_4}u(r)\frac{\partial\theta(r)}{\partial r} + \frac{M_0}{S_2}exp(-\beta r)u = 0, \tag{4}$$

Non-dimensionalized boundary conditions:

$$r = \eta: \quad u = 1, \quad \theta = 1,$$
$$r = 1: \quad u = 0, \quad \theta = 0.$$

where, $Ec = \frac{\rho_f(\omega r_1)^2}{(\rho C_p)_f \Delta T}$ is the Eckert number, $Re = \frac{\rho_f \omega r_1 r_2}{\mu_f}$ is the Reynolds number, $Pr = \frac{\mu_f(\rho C_p)_f}{\rho_f k_f}$ is the Prandtl number, $M_0 = \frac{\pi J M r_2^2}{8\mu_f \omega r_1}$, is the modified magnetic field parameter, $Rd = \frac{4\sigma_e T_c^3}{\beta_R k_f}$ is the radiation parameter, $F_r = \frac{r_2^2 r_1 \omega C_b}{\sqrt{K_1}\nu_f}$ is the Forchheimer number, $\beta = -\frac{\pi r_2}{a_0}$ is the exponential index parameter, $Da = \frac{r_2^2}{K_1}$ is the Darcy number, and $S_1 = \frac{\rho_{nf}}{\rho_f}, S_2 = \frac{\mu_{nf}}{\mu_f}, S_3 = \frac{(\rho C_p)_{nf}}{(\rho C_p)_f}, S_4 = \frac{k_{nf}}{k_f}$ are some constants associated with the thermal properties of hybrid nanofluids.

4. Numerical procedure

This study investigate the heat transfer in parabolic trough collectors due to hybrid nanofluid flow through the absorber tube with inserted rotating tube in the absorber. Equations governing the fluid flow dynamics are non-dimensionalized by incorporating the suitable similarity variables. The resulting non-dimensionalized equations governing the hybrid nanofluid flow are second-order, highly coupled, non-linear ordinary differential equations. And the numerical solutions of the these equations is tackled by the shooting technique with the combination of Adam Bashforth and Adam Moulten four step numerical approach, which uses both the explicit and implicit schemes to predict and correct the numerical solution, also known as the predictor–corrector method. The steps involved in numerical formulation of the current investigation are described below:

Governing equations:

$$u' = u_1,$$
$$u_2 = u_1' = -\frac{1}{r}u_1 + \frac{u}{r^2} + Re\frac{S_1}{S_2}uu_1 + \frac{M}{S_2}exp(-\beta r) + Dau + \frac{S_1}{S_2}F_r u^2,$$
$$\theta' = \theta_1,$$
$$\theta_2 = \theta_1' = \frac{1}{1+4Rd/3S_4}\left[PrRe\frac{S_3}{S_4}u\theta_1 - \frac{1}{r}\theta_1 - \frac{S_2}{S_4}EcPr\left[u_1 - \frac{1}{r}u\right]^2 - \frac{1}{S_4}PrEcMexp(-\beta r)u + (1+\frac{4Rd}{3S_4})\frac{1}{r}\theta_1\right]. \tag{5}$$

Boundary conditions:

$$r = \eta: \quad u = 1, \quad \theta = 1,$$
$$r = 1: \quad u = 0, \quad \theta = 0.$$

Adam Bashforth four step explicit (predictor) method for this system of first–order differential equation is written as:

$$u(1) = 1, \quad u_1(1) = t_1, \quad u_1(n+1) = 0, \quad \theta(1) = 1, \quad \theta_1(1) = g_1, \quad \theta(n+1) = 0.$$
$$u(k+1) = u(k) + \frac{h}{24}[55u_1(k) - 59u_1(k-1) + 37u_1(k-2) - 9u_1(k-3)],$$
$$u_1(k+1) = u_1(k) + \frac{h}{24}[55u_2(k) - 59u_2(k-1) + 37u_2(k-2) - 9u_2(k-3)],$$
$$\theta(k+1) = \theta(k) + \frac{h}{24}[55\theta_1(k) - 59\theta_1(k-1) + 37\theta_1(k-2) - 9\theta_1(k-3)],$$
$$\theta_1(k+1) = \theta_1(k) + \frac{h}{24}[55\theta_2(k) - 59\theta_2(k-1) + 37\theta_2(k-2) - 9\theta_2(k-3)]. \tag{6}$$

Adam Moulten four step implicit (corrector) method for this system of first–order differential equation is written as:

$$u(k+1) = u(k) + \frac{h}{720}[251u_1(k+1) + 646u_1(k) - 264u_1(k-1) + 106u_1(k-2) - 19u_1(k-3)],$$
$$u_1(k+1) = u_1(k) + \frac{h}{720}[251u_2(k+1) + 646u_2(k) - 264u_2(k-1) + 106u_2(k-2) - 19u_2(k-3)],$$
$$\theta(k+1) = \theta(k) + \frac{h}{720}[251\theta_1(k+1) + 646\theta_1(k) - 264\theta_1(k-1) + 106\theta_1(k-2) - 19\theta_1(k-3)],$$
$$\theta_1(k+1) = \theta_1(k) + \frac{h}{720}[251\theta_2(k+1) + 646\theta_2(k) - 264\theta_2(k-1) + 106\theta_2(k-2) - 19\theta_2(k-3)]. \tag{7}$$

where k varies from 4 to n, the first four steps of this numerical scheme are calculated by the Runga Kutta fourth-order method. The resulting momentum and energy equation are second-order ordinary differential equations. Therefore, we need two initial conditions for solving both the momentum and energy equations, but we have only one initial condition for both the momentum and energy equations. The remaining initial conditions for u_1 and θ_1 are calculated using the shooting technique by setting initial guesses t_1 and g_1 and updating them using Newton's method. The expression of Newton method for updating the initial guesses is given by:

$$t_1 = t_1 - \frac{u(b, n+1) - u(b)}{u_1(b, n+1)},$$
$$g_1 = g_1 - \frac{\theta(b, n+1) - \theta(b)}{\theta_1(b, n+1)},$$

where $u(b, n+1)$, $u_1(b, n+1)$, $\theta(b, n+1)$ and $\theta_1(b, n+1)$ are the respective predicted values from the numerical scheme at the endpoint, and $u(b)$ and $\theta(b)$ are the respective boundary conditions given at the end point of the domain. Initial guesses are updated continuously until the numerical solution converges to the error tolerance of 10^{-6} for both the momentum and energy equations.

$$u(b, n+1) - u(b) \leq 10^{-6}$$

$$\theta(b, n+1) - \theta(b) \leq 10^{-6}$$

5. Graphical results

This study numerically investigates the entropy generation and heat transfer in parabolic trough collectors due to hybrid nanofluid flow through the absorber tube with inserted rotating tube under the influences Darcy Forchheimer's porous medium and Riga surface. The governing equations representing the fluid flow dynamics are non-dimensionalized by incorporating the suitable similarity transformations. The numerical solutions of the resulting non-linear governing equations are tackled via the shooting technique in combination with Adam Bashforth and Adam Moulten's four-step numerical approach, which uses both the explicit and implicit fourth-order schemes to predict and correct the numerical solution, also known as the predictor–corrector method. Validation of the analysis is done with the article by Mohsenian et al. [54] by taking novel assumptions of this study as zero. Validation plots are plotted for the temperature and velocity profile results as shown in Fig. 2. These Figures report that this attempt is in good validation with the existing study.

5.1. Velocity profile results

Fig. 3 presents the results corresponding to the velocity profiles for diverse values of the different pertinent parameters. Fig. 3(a) illustrates the velocity profile affected by the modified magnetic field parameter M_0. Physically, the increasing effect of the magnetic field promotes a more vital Lorentz force to hybrid nanofluid flow, and a stronger Lorentz force reduces the drag coefficient at the surface, which diminishes the resulting nanofluid velocity. The influence of the exponential index of the Riga surface on the fluid velocity is picturized in Fig. 3(b). This picture presents that the fluid velocity is enhanced by escalating the exponential index parameter. An enhancing exponential index parameter weakens the strength of the applied magnetic field, diminishing the drag force and increasing the fluid velocity profile. Figs. 3(c) and 3(d) indicate the behavior of fluid velocity due to variation in Darcy number and Forchheimer number. In this Figure, it is displayed that the rise in the Darcy number and the Forchheimer number drops the velocity profile because the porosity of the medium resists the fluid flow, due to which the velocity profile worsens.

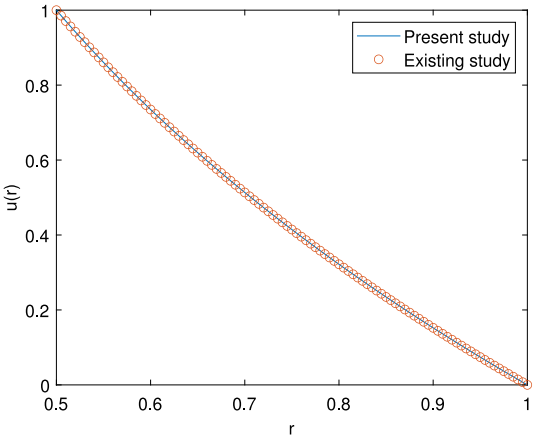

(a) Validation plot for the velocity profiles

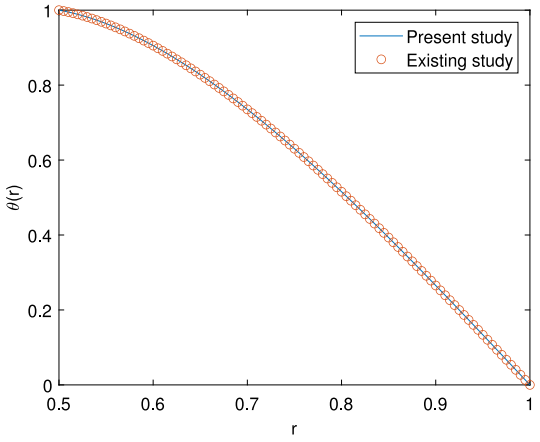

(b) Validation plots for the temperature profiles

Fig. 2. Present study validated with the study of Mohsenian et al. [54] in the Figs. 2(a) and 2(b).

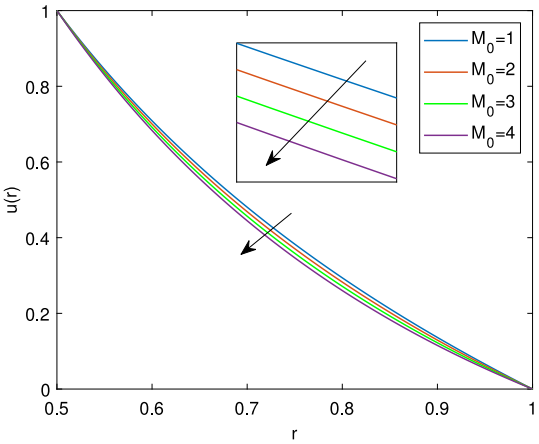

(a) Variation in $u(r)$ for different values of M_0

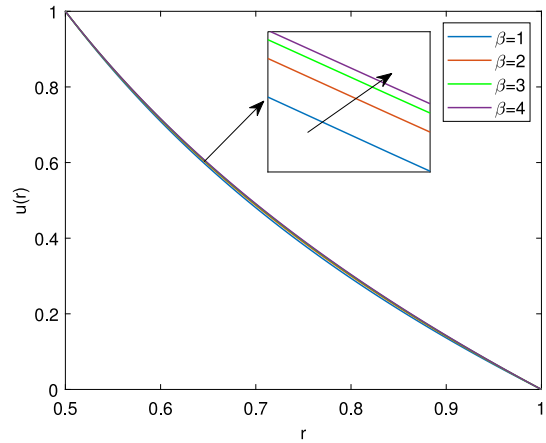

(b) $u(r)$ against diverse values of β

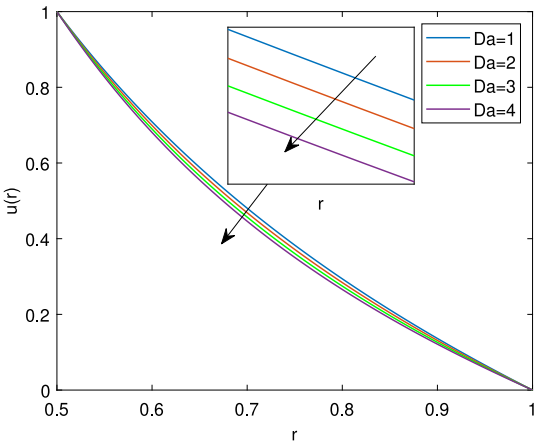

(c) Variation in $u(r)$ for different values of Da

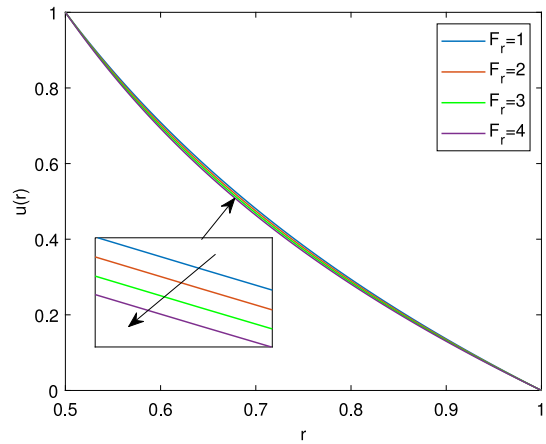

(d) $u(r)$ against diverse values of F_r

Fig. 3. Plots of velocity profiles for the diverse values of various influential physical parameters.

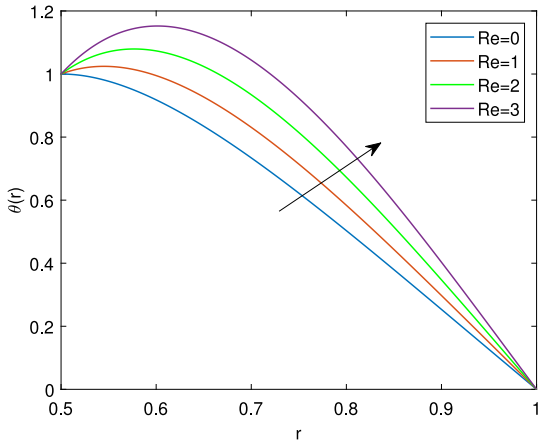

(a) $\theta(r)$ against diverse values of Re

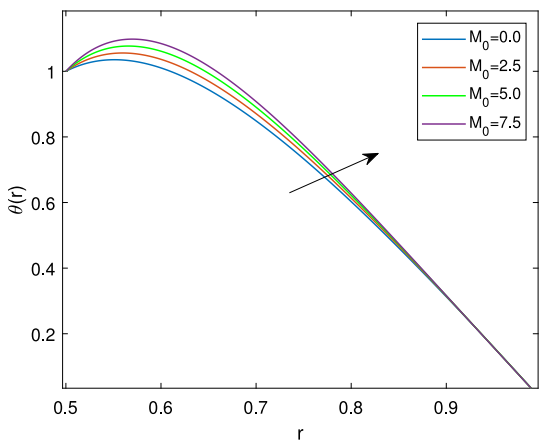

(b) $\theta(r)$ against diverse values of M_0

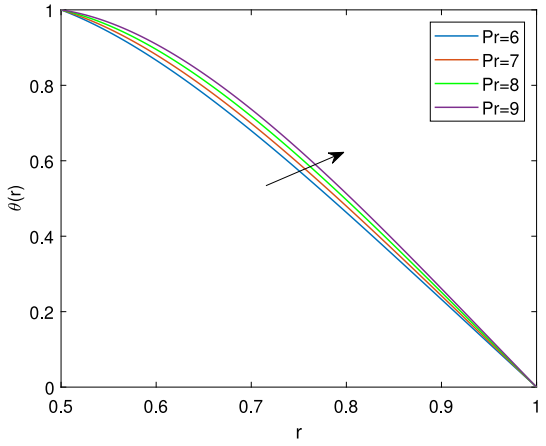

(c) $\theta(r)$ against diverse values of Pr

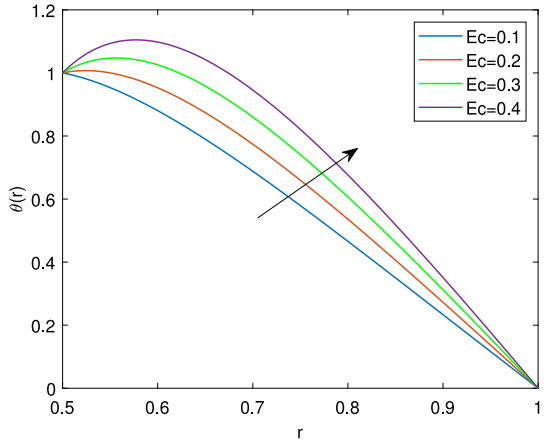

(d) $\theta(r)$ against diverse values of Ec

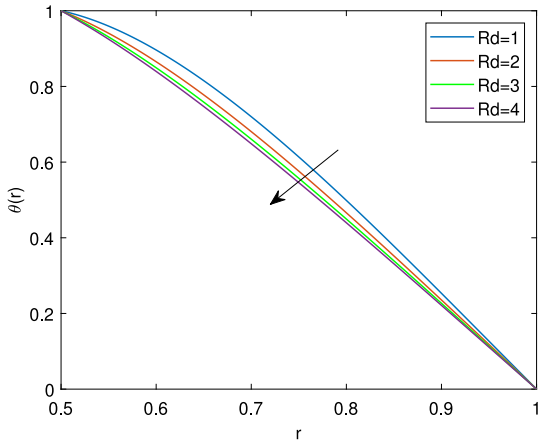

(e) $\theta(r)$ against diverse values of Rd

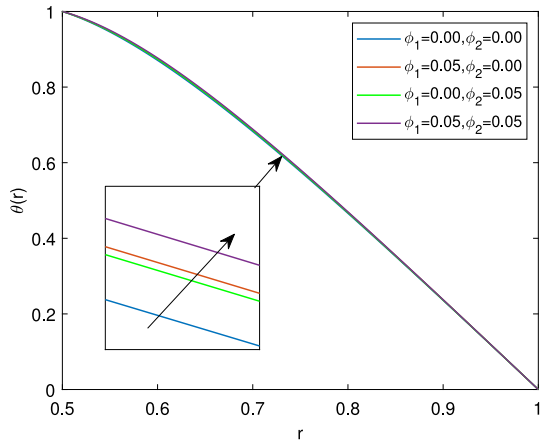

(f) $\theta(r)$ against diverse values of ϕ_1 and ϕ_2

Fig. 4. Plots representing the temperature profiles for diverse values of various pertinent parameters.

5.2. Thermal profiles results

Numerical findings of the fluid temperature profiles affected by the various physical parameters are displayed in Figs. 4. Fig. 4(a) represent the results of thermal profiles for diverse values of Reynolds number. This Figure reveals that the increment in Reynolds number increases the fluid temperature profile. An increasing Reynolds number increases the inertial forces in the fluid flow, improving fluid movement within the boundary layer and enhancing the thermal profiles. The modified magnetic field parameter results for the thermal profiles are presented in Fig. 4(b). In this Figure, it is seen that the fluid temperature profiles are enhanced with an enhancement in modified magnetic field parameters. A higher value of the modified magnetic field parameter means a more vital Lorentz force in the fluid, and the Lorentz force reduces the drag coefficient in the fluid flow, which enhances the interaction between the working fluid and the surface of the absorber tube due to which an improvement in thermal profiles achieved. Thermal profiles for the magnifying values of the Prandtl number are shown in Fig. 4(c). This Figure reports that the temperature profiles are enhanced due to enhancing the Prandtl number. A higher Prandtl number indicates that the fluid has a higher ability to conduct heat relative to its ability to convect it. In such cases, heat tends to conduct away from the heated surface more efficiently, leading to changes in temperature profiles. Fig. 4(d) presents the influence of the Eckert number on fluid temperature profiles, showing that an enhanced Eckert number augments the thermal profiles. Eckert number quantifies the ratio of the kinetic energy of the fluid to the thermal energy changes within the flow. Enhancing the Eckert number indicates more kinetic energy in the fluid flow, leading to increased mixing and better heat transfer. The increased turbulence and mixing within the fluid results in better heat dispersion and reduced temperature gradients. Results of the thermal profiles for the radiation parameter are reported in Fig. 4(e). As per this Figure, it is seen that the thermal profiles reduces for enhancing the radiation parameter, and this result has a similar trend with the findings of the existing literature [55]. Fig. 4(f) illustrates the outcomes of thermal profile results due to distinct volume concentrations of the nanoparticles. The first case is plotted for thermal profile results due to the base fluid Therminol-VPI by taking nanoparticle concentrations as $\phi_1 = 0.00$, $\phi_2 = 0.00$. The second and third cases are plotted for the thermal profiles obtained due to the nanofluids by taking nanoparticles concentrations $\phi_1 = 0.05$, $\phi_2 = 0.00$ and $\phi_1 = 0.00$, $\phi_2 = 0.05$, and the fourth case is plotted for the thermal profile due to the hybrid nanofluid with nanoparticles concentrations $\phi_1 = 0.05$, $\phi_2 = 0.05$. This Figure shows that thermal profiles due to hybrid nanofluids are higher than the nanofluids. And, the thermal profiles of the nanofluids are higher than the base fluid. Also, the thermal profiles for alumina nanoparticle-based nanofluid are higher than the multi-walled-carbon-nanotube-based nanofluid.

6. Quantity of engineering interest

In parabolic solar collectors, the physical quantity of engineering interest is the heat transfer rate, i.e., the Nusselt number. Our main objective is to augments the efficiency of concentrated solar power technology by enhancing heat transfer in the working fluid by introducing new terminologies, which allow storing more thermal energy from incoming solar radiation to meet the sustainable energy demand. Therefore, the Nusselt number is defined as.

$$Nu = -S_4\left(1 + \frac{4Rd}{3S_4}\right)\frac{\partial\theta}{\partial r}|_{r=\eta}$$

Figs. 5 presents the numerical findings obtained for the Nusselt number against different physical parameters. Fig. 5(a) show the Nusselt number results against the Prandtl number for different values of modified magnetic field parameters. According to this Figure, it is noted that the Nusselt number reduces with increase in the Prandtl number and modified magnetic field parameter. Fig. 5(b) present the Nusselt number influenced by the Reynolds number for diverse values of the exponential index. This Figure reports that augmenting the Reynolds number drops the Nusselt number, and it grows by escalating the exponential index parameter. Findings of the Nusselt number due to radiation parameters for the varying values of the Eckert number are picturized in Fig. 5(c). This Figure illustrates that the Nusselt number escalates with a rise in radiation parameter and decelerates with an improvement in the Eckert number. The influences of Darcy number and Forchheimer parameter on Nusselt number are presented in Fig. 5(d). This Figure shows that a rise in Darcy and Forchheimer decreases the Nusselt number. Fig. 5(e) presents the Nusselt number, i.e., heat transfer rate results for the Therminol-VPI based fluid, aluminum-oxide nanofluid, multiwalled carbon nanotube based nanofluid, and hybrid nanofluid. This Figure shows that nanofluids have higher heat transfer rates than the conventional Therminol-VPI base fluid, and hybrid nanofluids have higher heat transfer rates than both the aluminum-oxide (Al_2O_3) and multiwalled carbon nanotube (MWCNT) nanofluids at the same nanoparticle volume fraction.

7. Entropy optimization

Heat loss in an irreversible process in a thermodynamic system is called entropy generation. To evaluate the performance of the thermodynamic system, it is compulsory to examine the heat loss in the irreversible process. Entropy is generated in this model through conductive heat transfer, viscous dissipation, nanoparticle diffusion, Darcy Forchheimer porous media, and the Riga surface. The mathematical term for entropy generation is:

$$E_g = \frac{1}{T_2^2}\left(\kappa_{hnf} + \frac{16\sigma^* T_2^3}{3\kappa^*(\rho c_p)_{hnf}}\right)\left(\frac{\partial T}{\partial R}\right)^2 + \frac{\mu_{hnf}}{T_2}\left(\frac{\partial U}{\partial R} + \frac{U}{R}\right)^2 + \frac{\pi J M}{\rho_{hnf}} exp(-\frac{\pi}{a_0}R)U + \nu_{hnf}\frac{U^2}{K_1} + \frac{C_b}{\sqrt{K_1}}U^3 \quad (8)$$

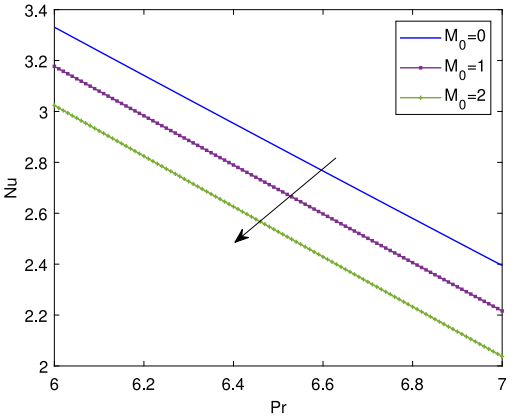

(a) Nusselt number against Pr for diverse values of M_0

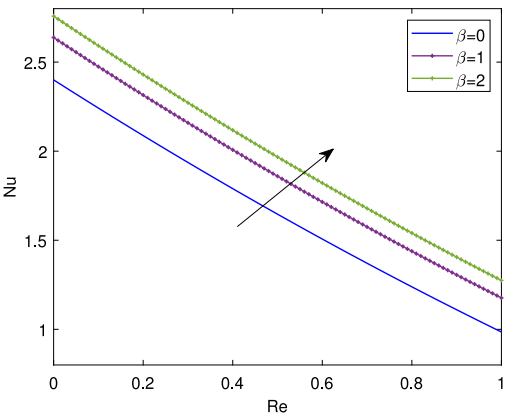

(b) Nusselt number against Re for diverse values of β

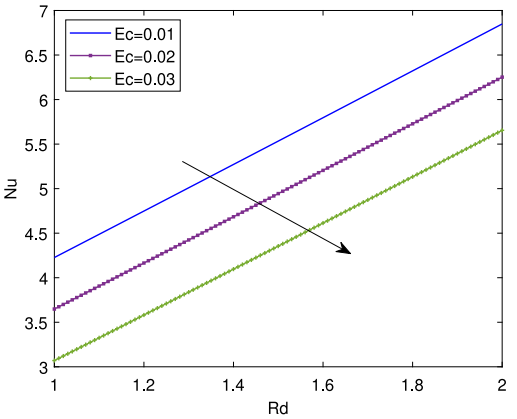

(c) Nusselt number against Rd for diverse values of Ec

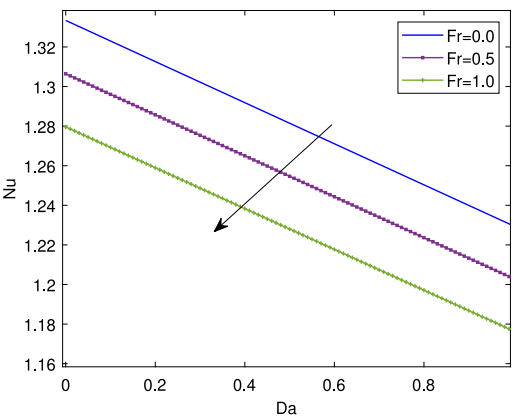

(d) Nusselt number against Fr for diverse values of Da

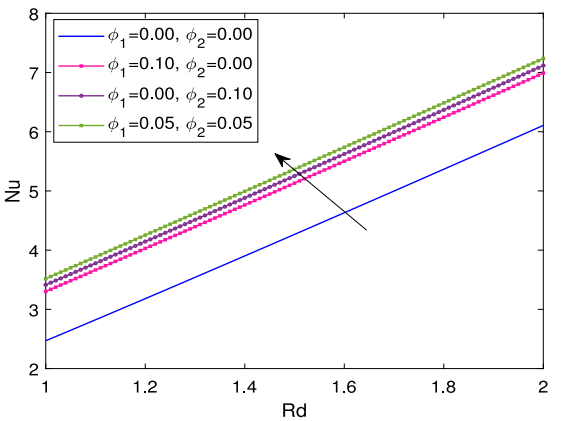

(e) Nusselt number for fluid (ϕ_1 = 0.00, ϕ_2 = 0.00), Al_2O_3-nanofluid (ϕ_1 = 0.10, ϕ_2 = 0.00), $MWCNT$-nanofluid (ϕ_1 = 0.00, ϕ_2 = 0.10) and hybrid nanofluid (ϕ_1 = 0.05, ϕ_2 = 0.05)

Fig. 5. Plots of Nusselt number for diverse values of different influential parameters.

After introducing dimensionless variables, the non-dimensionalized form of the expression for entropy generation is as follows:

$$N_s = \left(1+\frac{4Rd}{3S_4}\right)\left(\frac{\partial\theta}{\partial r}\right)^2 + \delta EcPr\frac{S_2}{S_4}\left[\frac{\partial u(r)}{\partial r} - \frac{1}{r}u(r)\right]^2 + \frac{1}{S_4}\delta PrEcMexp(-Br)u(r) + \frac{S_2}{S_4}\delta PrEcDau(r)^2 + \frac{1}{S_4}\delta PrEcFru(r)^3$$

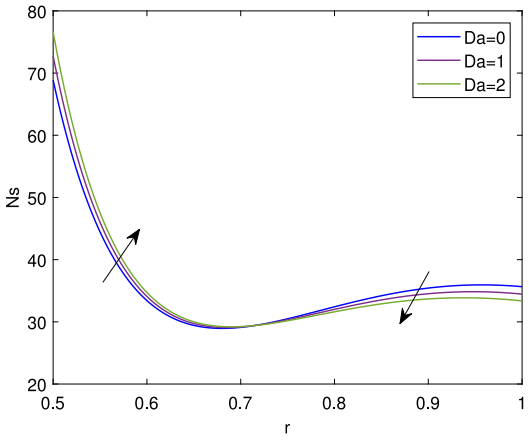

(a) Entropy formation against Darcy number

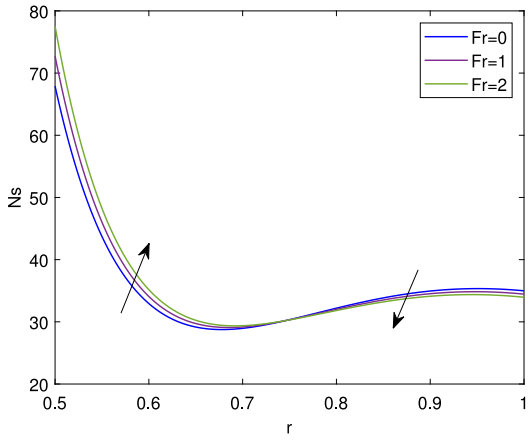

(b) Entropy formation against Forchheimer parameter

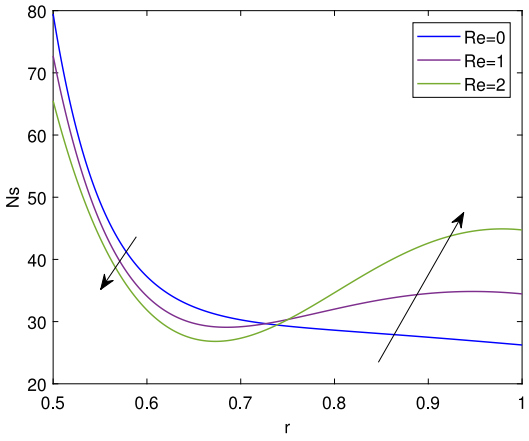

(c) Entropy formation against Reynolds number

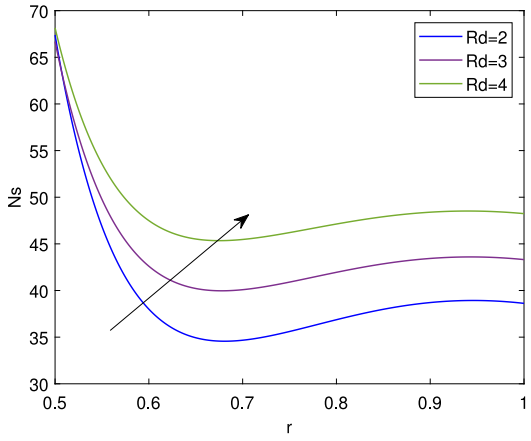

(d) Entropy formation against radiation number

Fig. 6. Plots of entropy formation against different influential parameters.

Entropy generation determines the heat losses in the thermal systems due to irreversibilities in the heat transfer processes. Minimization of the overall entropy in the thermal systems improves the performance and efficiency of the thermal systems. Figs. 6 presents the entropy generation results influenced by the different physical parameters. Figs. 6(a) and 6(b) demonstrate the entropy generation due to the variation in Forchheimer number and Darcy number. In these figures, it is seen that the entropy generation result shows a dual behavior for the varying values of the Darcy and Forchheimer numbers, having the same trends for both the Darcy and Forchheimer numbers. Entropy generation first rises with a rise in both the Darcy and Forchheimer numbers, and near the midpoint of the similarity variable, entropy generation changes reduce with escalating Darcy and Forchheimer numbers. Entropy generation influenced by Reynolds number is depicted in Fig. 6(c). This Figure clears that entropy generation first diminishes with an enhancement in Reynolds number and than after the mid point of the similarity variable entropy generation enhances with escalating Reynolds number. Fig. 6(d) displays the entropy generation due to variation in radiation parameter. As per this Figure it is noted that entropy generation magnifies by enhancing the radiation parameter.

8. Conclusions

This attempt analyzed the heat transfer and entropy generation in hybrid-nanofluid flow due to a rotating tube in the absorber under the influence of the Darcy-Forchheimer porous medium and Riga surface. The governing equations are non-dimensionalized with the help of similarity variables. The numerical investigation of the proposed mathematical model for the resulting dimensionless coupled ordinary differential equations is done by Adams Bashforth and Adams Moulten's four-step method with the shooting technique. Newton's method is used to update the initial guesses. The main concluding remarks of the current investigation are listed below:

- Fluid velocity reduces with the rise in the modified magnetic field parameter M_0, and the velocity profiles $u(r)$ accelerates with the rise in the exponential index parameter β.
- Velocity profile diminishes with escalates in Forchheimer number F_r and Darcy number Da.
- Thermal profiles $\theta(r)$ enhances with an improvement in Reynold's number Re, modified magnetic field parameter M_0, Prandtl number Pr, and Eckert number Ec, and thermal profiles $\theta(r)$ reduce with growing the radiation parameter Rd.
- Nusselt number Nu_x decreases with augmenting values of Eckert number Ec, modified magnetic field parameter M_0, Darcy number Da, Prandtl number Pr, and Forchheimer number F_r.
- Nusselt number enhances by magnifying the exponential index parameter β, and radiation parameter Rd.
- Entropy generation first rises with a rise in the Forchheimer number F_r and Darcy number Da. And, after the midpoint of the similarity variable, entropy reduces with escalates in the Forchheimer number F_r and Darcy number Da.
- Entropy generation first decelerates with an escalating in Reynolds number Re and then after the midpoint of the similarity variable it enhances with an increment in Reynolds number Re.
- Entropy generation escalates by enhancing the radiation parameter Rd.

Utilizing solar energy is regarded as the effective solution for addressing current energy requirements and environmental issues, such as the depletion of fossil fuels and global warming. Parabolic trough solar collectors are the most demonstrated collectors for capturing the concentrated solar radiation in solar power generation. Riga plate is usually employed to enhance the fluid's thermophysical characteristics and prevent mechanical energy loss. The Riga plate device generates magneto-electric fields. The external magnetic and electric field's strength has a specific external element that controls fluid flow and minimizes drag force. All thermofluidic processes involve irreversibilities, resulting in a loss of efficiency. In practice, the entropy formation calculates the irreversibilities to minimize the entropy generation rate and maximize accessible energy.

Nomenclature

a_0 represents the width of magnets and electrodes, (m)	Da is the Darcy number
F is the Lorentz force ($N = \text{kg m s}^{-2}$)	Ec Eckert number
M is the strength of the magnets ($T = \text{kg s}^{-2}\ \text{A}^{-1}$)	Fr is the Forchheimer number
C_p specific heat capacity at constant pressure ($\text{J K}^{-1}\ \text{kg}^{-1}$)	c_b drag coefficient independent of viscosity
k is the thermal conductivity ($\text{W m}^{-1}\ \text{K}^{-1}$)	J represents the current density by the electrodes. (NC^{-1})
M_0 is modified magnetic field parameter	K_1 permeability of the medium, (m^2)
q_r is the strength of non-linear radiation	Pr Prandtl number
T_1 is the temperature of inner tube (K)	T is the temperature (K)
U is the velocity component in radial direction (m s^{-1})	T_2 is the temperature of external tube (K)
r_1 is the radius of inner tube (m)	u is dimensionless velocity
R is the radial direction (m)	r is dimensionless radius
Re Reynolds number	r_2 is the radius of absorber tube (m)
μ dynamic viscosity ($\text{kg m}^{-1}\ \text{s}^{-1}$.)	Rd is the radiation parameter
ω is the rotational velocity (rad s^{-1})	β is the exponential index parameter
σ electrical conductivity (S m^{-1})	ν is the kinematic viscosity ($\text{m}^2\ \text{s}^{-1}$)
ϕ_1 is the concentration of aluminum-oxide nanoparticles	ρ is the hybrid nanofluid density, (kg m^{-3})
Suffixes	θ is the dimensionless temperature
nf represent nanofluid	ϕ_2 is the concentration of multi-walled carbon-nanotube nanoparticles
	hnf represent hybrid nanofluid
	f represent fluid

CRediT authorship contribution statement

B.K. Sharma: Project administration, Investigation, Resources, Writing – original draft. **Anup Kumar:** Conceptualization, Methodology, Software, Formal analysis, Writing – original draft. **Bandar Almohsen:** Methodology, Software, Formal analysis. **Unai Fernandez-Gamiz:** Software, Funding acquisition, Supervision.

Declaration of competing interest

The authors declare that they have no known competing financial interests or personal relationships that could have appeared to influence the work reported in this paper.

Data availability

No data was used for the research described in the article.

Acknowledgments

Author U.F.-G. appreciates the support of the Government of the Basque Country, Grant N. ELKARTEK 22/85 and ELKARTEK 21/10. The research is supported by Researchers Supporting Project number (RSP2023R158), King Saud University, Riyadh, Saudi Arabia.

References

[1] R.V. Padilla, G. Demirkaya, D.Y. Goswami, E. Stefanakos, M.M. Rahman, Heat transfer analysis of parabolic trough solar receiver, Appl. Energy 88 (12) (2011) 5097–5110.
[2] C. Albanakis, D. Missirlis, N. Michailidis, K. Yakinthos, A. Goulas, H. Omar, D. Tsipas, B. Granier, Experimental analysis of the pressure drop and heat transfer through metal foams used as volumetric receivers under concentrated solar radiation, Exp. Therm Fluid Sci. 33 (2) (2009) 246–252.
[3] L. Jianfeng, D. Jing, Y. Jianping, Heat transfer performance of an external receiver pipe under unilateral concentrated solar radiation, Sol. Energy 84 (11) (2010) 1879–1887.
[4] X. Chen, X.-L. Xia, H. Liu, Y. Li, B. Liu, Heat transfer analysis of a volumetric solar receiver by coupling the solar radiation transport and internal heat transfer, Energy Convers. Manage. 114 (2016) 20–27.
[5] W. Lipiński, E. Abbasi-Shavazi, J. Chen, J. Coventry, M. Hangi, S. Iyer, A. Kumar, L. Li, S. Li, J. Pye, et al., Progress in heat transfer research for high-temperature solar thermal applications, Appl. Therm. Eng. 184 (2021) 116137.
[6] A. Pantokratoras, E. Magyari, EMHD free-convection boundary-layer flow from a Riga-plate, J. Eng. Math. 64 (3) (2009) 303–315.
[7] M. Ayub, T. Abbas, M. Bhatti, Inspiration of slip effects on electromagnetohydrodynamics (EMHD) nanofluid flow through a horizontal Riga plate, Eur. Phys. J. Plus 131 (6) (2016) 1–9.
[8] R. Ahmad, M. Mustafa, M. Turkyilmazoglu, Buoyancy effects on nanofluid flow past a convectively heated vertical Riga-plate: A numerical study, Int. J. Heat Mass Transfer 111 (2017) 827–835.
[9] A. Shafiq, Z. Hammouch, A. Turab, Impact of radiation in a stagnation point flow of Walters' B fluid towards a Riga plate, Therm. Sci. Eng. Prog. 6 (2018) 27–33.
[10] G. Rasool, T. Zhang, A. Shafiq, Second grade nanofluidic flow past a convectively heated vertical Riga plate, Phys. Scr. 94 (12) (2019) 125212.
[11] K. Ramesh, S.U. Khan, M. Jameel, M.I. Khan, Y.-M. Chu, S. Kadry, Bioconvection assessment in Maxwell nanofluid configured by a Riga surface with nonlinear thermal radiation and activation energy, Surf. Interfaces 21 (2020) 100749.
[12] K.K. Asogwa, S.M. Bilal, I.L. Animasaun, F.M. Mebarek-Oudina, Insight into the significance of ramped wall temperature and ramped surface concentration: The case of casson fluid flow on an inclined Riga plate with heat absorption and chemical reaction, Nonlinear Eng. 10 (1) (2021) 213–230.
[13] B.K. Sharma, U. Khanduri, N.K. Mishra, A.J. Chamkha, Analysis of arrhenius activation energy on magnetohydrodynamic gyrotactic microorganism flow through porous medium over an inclined stretching sheet with thermophoresis and Brownian motion, Proc. Inst. Mech. Eng. E (2022) 09544089221128768.
[14] B. Sharma, R. Gandhi, M. Bhatti, Entropy analysis of thermally radiating MHD slip flow of hybrid nanoparticles (Au-Al2O3/blood) through a tapered multi-stenosed artery, Chem. Phys. Lett. 790 (2022) 139348.
[15] R. Ghandi, B. Sharma, C. Kumawat, O. Beg, et al., Modeling and analysis of magnetic hybrid nanoparticle (Au-Al2O3/blood) based drug delivery through a bell-shaped occluded artery with joule heating, viscous dissipation and variable viscosity effects, Proc. Inst. Mech. Eng. E (2022).
[16] B. Sharma, A. Kumar, R. Gandhi, M. Bhatti, Exponential space and thermal-dependent heat source effects on electro-magneto-hydrodynamic Jeffrey fluid flow over a vertical stretching surface, Internat. J. Modern Phys. B 36 (30) (2022) 2250220.
[17] N. Sultana, S. Shaw, M.K. Nayak, S. Mondal, Hydromagnetic slip flow and heat transfer treatment of Maxwell fluid with hybrid nanostructure: low Prandtl numbers, Int. J. Ambient Energy 44 (1) (2023) 947–957.
[18] D. Mohanty, G. Mahanta, S. Shaw, M. Das, Thermosolutal marangoni stagnation point GO–MoS2/water hybrid nanofluid over a stretching sheet with the inclined magnetic field, Internat. J. Modern Phys. B (2023) 2450024.
[19] A.J. Chamkha, C. Issa, K. Khanafer, Natural convection from an inclined plate embedded in a variable porosity porous medium due to solar radiation, Int. J. Therm. Sci. 41 (1) (2002) 73–81.
[20] F. Wang, Y. Shuai, H. Tan, C. Yu, Thermal performance analysis of porous media receiver with concentrated solar irradiation, Int. J. Heat Mass Transfer 62 (2013) 247–254.
[21] F. Wang, J. Tan, Z. Wang, Heat transfer analysis of porous media receiver with different transport and thermophysical models using mixture as feeding gas, Energy Convers. Manage. 83 (2014) 159–166.
[22] L.A. Soltani, E. Shivanian, R. Ezzati, Convection–radiation heat transfer in solar heat exchangers filled with a porous medium: Exact and shooting homotopy analysis solution, Appl. Therm. Eng. 103 (2016) 537–542.
[23] O.A. Bég, N. Ali, A. Zaman, E.T. Bég, A. Sohail, Computational modeling of heat transfer in an annular porous medium solar energy absorber with the P1-radiative differential approximation, J. Taiwan Inst. Chem. Eng. 66 (2016) 258–268.
[24] S. Rashidi, J.A. Esfahani, A. Rashidi, A review on the applications of porous materials in solar energy systems, Renew. Sustain. Energy Rev. 73 (2017) 1198–1210.
[25] B.G. Lougou, Y. Shuai, R. Pan, G. Chaffa, H. Tan, Heat transfer and fluid flow analysis of porous medium solar thermochemical reactor with quartz glass cover, Int. J. Heat Mass Transfer 127 (2018) 61–74.
[26] M. Luo, C. Wang, J. Zhao, L. Liu, Characteristics of effective thermal conductivity of porous materials considering thermal radiation: A pore-level analysis, Int. J. Heat Mass Transfer 188 (2022) 122597.
[27] B. Sharma, R. Gandhi, Combined effects of joule heating and non-uniform heat source/sink on unsteady MHD mixed convective flow over a vertical stretching surface embedded in a Darcy-forchheimer porous medium, Propul. Power Res. 11 (2) (2022) 276–292.
[28] M. Firoozzadeh, M. Shafiee, Thermodynamic analysis on using titanium oxide/oil nanofluid integrated with porous medium in an evacuated tube solar water heater, J. Therm. Anal. Calorim. (2023) 1–14.
[29] D. Mohanty, N. Sethy, G. Mahanta, S. Shaw, Impact of the interfacial nanolayer on marangoni convective Darcy–Forchheimer hybrid nanofluid flow over an infinite porous disk with Cattaneo–Christov heat flux, Therm. Sci. Eng. Prog. 41 (2023) 101854.
[30] X. Li, G. Zeng, X. Lei, The stability, optical properties and solar-thermal conversion performance of SiC-MWCNTs hybrid nanofluids for the direct absorption solar collector (DASC) application, Sol. Energy Mater. Sol. Cells 206 (2020) 110323.
[31] M.H. Ahmadi, M. Ghazvini, M. Sadeghzadeh, M.A. Nazari, M. Ghalandari, Utilization of hybrid nanofluids in solar energy applications: a review, Nano-Struct. Nano-Objects 20 (2019) 100386.
[32] Q. Xiong, S. Altnji, T. Tayebi, M. Izadi, A. Hajjar, B. Sundén, L.K. Li, A comprehensive review on the application of hybrid nanofluids in solar energy collectors, Sustain. Energy Technol. Assess. 47 (2021) 101341.
[33] G. Hu, X. Ning, M. Hussain, U. Sajjad, M. Sultan, H.M. Ali, T.R. Shah, H. Ahmad, Potential evaluation of hybrid nanofluids for solar thermal energy harvesting: A review of recent advances, Sustain. Energy Technol. Assess. 48 (2021) 101651.

[34] K.G. Kumar, E.H.B. Hani, M.E.H. Assad, M. Rahimi-Gorji, S. Nadeem, A novel approach for investigation of heat transfer enhancement with ferromagnetic hybrid nanofluid by considering solar radiation, Microsyst. Technol. 27 (2021) 97–104.
[35] H. Adun, M. Adedeji, V. Adebayo, A. Shefik, O. Bamisile, D. Kavaz, M. Dagbasi, Multi-objective optimization and energy/exergy analysis of a ternary nanofluid based parabolic trough solar collector integrated with kalina cycle, Sol. Energy Mater. Sol. Cells 231 (2021) 111322.
[36] M. Abid, M.S. Khan, T.A.H. Ratlamwala, M.N. Malik, H.M. Ali, Q. Cheok, Thermodynamic analysis and comparison of different absorption cycles driven by evacuated tube solar collector utilizing hybrid nanofluids, Energy Convers. Manage. 246 (2021) 114673.
[37] A.K. Tiwari, V. Kumar, Z. Said, H. Paliwal, A review on the application of hybrid nanofluids for parabolic trough collector: Recent progress and outlook, J. Clean. Prod. 292 (2021) 126031.
[38] R. Gandhi, B.K. Sharma, O.D. Makinde, Entropy analysis for MHD blood flow of hybrid nanoparticles (Au–Al2O3/blood) of different shapes through an irregular stenosed permeable walled artery under periodic body acceleration: Hemodynamical applications, ZAMM-J. Appl. Math. Mech./Z. Angew. Math. Mech. (2022) e202100532.
[39] M. Tavakoli, M.R. Soufivand, Investigation of entropy generation, PEC, and efficiency of parabolic solar collector containing water/Al2O3- MWCNT hybrid nanofluid in the presence of finned and perforated twisted tape turbulators using a two-phase flow scheme, Eng. Anal. Bound. Elem. 148 (2023) 324–335.
[40] Y. Tong, T. Boldoo, J.H. Mr, H. Cho, Improvement of photo-thermal energy conversion performance of MWCNT/Fe3O4 hybrid nanofluid compared to Fe3O4 nanofluid, Energy 196 (2020) 117086.
[41] Y. Khetib, K. Sedraoui, A.A. Melaibari, R. Alsulami, The numerical investigation of spherical grooves on thermal–hydraulic behavior and exergy efficiency of two-phase hybrid MWCNT-Al2O3/water nanofluid in a parabolic solar collector, Sustain. Energy Technol. Assess. 47 (2021) 101530.
[42] E. Elshazly, I. El-Mahallawi, et al., Thermal performance enhancement of evacuated tube solar collector using MWCNT, Al2O3, and hybrid MWCNT/Al2O3 nanofluids, Int. J. Thermofluids 17 (2023) 100260.
[43] R. Gope, M.K. Nayak, S. Shaw, S. Mondal, Hydro-thermo-fluidic aspects of oldroyd b fluid with hybrid nanostructure subject to low and moderate Prandtl numbers, Multidiscip. Model. Mater. Struct. 19 (2) (2023) 292–310.
[44] S. Parvin, R. Nasrin, M. Alim, Heat transfer and entropy generation through nanofluid filled direct absorption solar collector, Int. J. Heat Mass Transfer 71 (2014) 386–395.
[45] M. Charjouei Moghadam, M. Edalatpour, J.P. Solano, Numerical study on conjugated laminar mixed convection of alumina/water nanofluid flow, heat transfer, and entropy generation within a tube-on-sheet flat plate solar collector, J. Solar Energy Eng. 139 (4) (2017) 041011.
[46] M. Nayak, A.A. Hakeem, B. Ganga, M.I. Khan, M. Waqas, O.D. Makinde, Entropy optimized MHD 3D nanomaterial of non-Newtonian fluid: a combined approach to good absorber of solar energy and intensification of heat transport, Comput. Methods Programs Biomed. 186 (2020) 105131.
[47] W.-W. Wang, Y. Cai, L. Wang, C.-W. Liu, F.-Y. Zhao, M.A. Sheremet, D. Liu, A two-phase closed thermosyphon operated with nanofluids for solar energy collectors: Thermodynamic modeling and entropy generation analysis, Sol. Energy 211 (2020) 192–209.
[48] B. Sharma, R. Gandhi, N.K. Mishra, Q.M. Al-Mdallal, Entropy generation minimization of higher-order endothermic/exothermic chemical reaction with activation energy on MHD mixed convective flow over a stretching surface, Sci. Rep. 12 (1) (2022) 1–18.
[49] C. Kumawat, B. Sharma, Q.M. Al-Mdallal, M. Rahimi-Gorji, Entropy generation for MHD two phase blood flow through a curved permeable artery having variable viscosity with heat and mass transfer, Int. Commun. Heat Mass Transfer 133 (2022) 105954.
[50] R. Goyal, K. Reddy, Numerical investigation of entropy generation in a solar parabolic trough collector using supercritical carbon dioxide as heat transfer fluid, Appl. Therm. Eng. 208 (2022) 118246.
[51] B.K. Sharma, A. Kumar, R. Gandhi, M.M. Bhatti, N.K. Mishra, Entropy generation and thermal radiation analysis of EMHD Jeffrey nanofluid flow: Applications in solar energy, Nanomaterials 13 (3) (2023) 544.
[52] S.S.S. Sen, R. Mahato, S. Shaw, M. Das, Simulation of entropy and heat and mass transfer in water-EG based hybrid nanoliquid flow with MHD and nonlinear radiation, Numer. Heat Transfer A (2023) 1–15.
[53] D. Mohanty, G. Mahanta, S. Shaw, Analysis of irreversibility for 3-D MHD convective Darcy–Forchheimer Casson hybrid nanofluid flow due to a rotating disk with Cattaneo–Christov heat flux, Joule heating, and nonlinear thermal radiation, Numer. Heat Transfer B 84 (2) (2023) 115–142.
[54] S. Mohsenian, S. Gouran, S. Ghasemi, Evaluation of weighted residual methods for thermal radiation on nanofluid flow between two tubes in presence of magnetic field, Case Stud. Therm. Eng. 32 (2022) 101867.
[55] A. Wakif, A. Chamkha, I. Animasaun, M. Zaydan, H. Waqas, R. Sehaqui, Novel physical insights into the thermodynamic irreversibilities within dissipative EMHD fluid flows past over a moving horizontal Riga plate in the coexistence of wall suction and joule heating effects: a comprehensive numerical investigation, Arab. J. Sci. Eng. 45 (2020) 9423–9438.